



OPEN ACCESS

EDITED BY
Isidre Ferrer,
University of Barcelona, Spain

REVIEWED BY
Tong Li,
Johns Hopkins University,
United States
Diego Sepulveda-Falla,
University Medical Center
Hamburg-Eppendorf, Germany

*CORRESPONDENCE
Keping Chai
ckpzjy@126.com
Feng Wan
wanruiyan@hotmail.com
Jiawei Liang
D201980525@hust.edu.cn
Daojiang Shen
zjyysdj@126.com

†These authors have contributed
equally to this work

SPECIALTY SECTION
This article was submitted to
Alzheimer's Disease and Related
Dementias,
a section of the journal
Frontiers in Aging Neuroscience

RECEIVED 17 December 2021
ACCEPTED 30 May 2022
PUBLISHED 13 July 2022

CITATION
Chai K, Zhang X, Chen S, Gu H, Tang H,
Cao P, Wang G, Ye W, Wan F, Liang J
and Shen D (2022) Application of
weighted co-expression network
analysis and machine learning to
identify the pathological mechanism
of Alzheimer's disease.
Front. Aging Neurosci. 14:837770.
doi: 10.3389/fnagi.2022.837770

COPYRIGHT
© 2022 Chai, Zhang, Chen, Gu, Tang,
Cao, Wang, Ye, Wan, Liang and Shen.
This is an open-access article
distributed under the terms of the
[Creative Commons Attribution License
\(CC BY\)](https://creativecommons.org/licenses/by/4.0/). The use, distribution or
reproduction in other forums is
permitted, provided the original
author(s) and the copyright owner(s)
are credited and that the original
publication in this journal is cited, in
accordance with accepted academic
practice. No use, distribution or
reproduction is permitted which does
not comply with these terms.

Application of weighted co-expression network analysis and machine learning to identify the pathological mechanism of Alzheimer's disease

Keping Chai^{1*†}, Xiaolin Zhang^{2†}, Shufang Chen¹,
Huaqian Gu¹, Huitao Tang¹, Panlong Cao¹,
Gangqiang Wang¹, Weiping Ye¹, Feng Wan^{2*}, Jiawei Liang^{3*}
and Daojiang Shen^{1*}

¹Department of Pediatrics, Zhejiang Hospital, Hangzhou, China, ²Department of Neurological Surgery, Tongji Hospital, Tongji Medical College, Huazhong University Science and Technology, Wuhan, China, ³College of Life Science and Technology, Huazhong University of Science and Technology, Wuhan, China

Aberrant deposits of neurofibrillary tangles (NFT), the main characteristic of Alzheimer's disease (AD), are highly related to cognitive impairment. However, the pathological mechanism of NFT formation is still unclear. This study explored differences in gene expression patterns in multiple brain regions [entorhinal, temporal, and frontal cortex (EC, TC, FC)] with distinct Braak stages (0- VI), and identified the hub genes *via* weighted gene co-expression network analysis (WGCNA) and machine learning. For WGCNA, consensus modules were detected and correlated with the single sample gene set enrichment analysis (ssGSEA) scores. Overlapping the differentially expressed genes (DEGs, Braak stages 0 vs. I-VI) with that in the interest module, metascape analysis, and Random Forest were conducted to explore the function of overlapping genes and obtain the most significant genes. We found that the three brain regions have high similarities in the gene expression pattern and that oxidative damage plays a vital role in NFT formation *via* machine learning. Through further filtering of genes from interested modules by Random Forest, we screened out key genes, such as LYN, LAPTM5, and IFI30. These key genes, including LYN, LAPTM5, and ARHGDB, may play an important role in the development of AD through the inflammatory response pathway mediated by microglia.

KEYWORDS

Braak stages, random forest, WGCNA, ssGSEA, neurodegeneration

Introduction

Via the distribution of neurofibrillary tangles (NFT) in the brain, Braak stages can not only be used for the pathological classification of Alzheimer's disease (AD) (Dickson, 1997), they are also related to memory and intellectual performance. However, to date, the pathological mechanism of NFT formation is still unclear (Duyckaerts et al., 1997; Grober et al., 1999). A large body of evidence indicates that at different stages of AD,

the distribution region of NFT in the brain is also different. For example, the entorhinal cortex (EC) is the area where NFT deposits occur first in AD (Braak and Braak, 1991). However, the pathological mechanism of its formation is still unclear. Several hypotheses, such as oxidative damage, oxidative stress, insulin resistance, apoE, neuroinflammation, and other theories were established (Solomon et al., 2014; Nakamura et al., 2018). Exploring the gene expression patterns of different brain regions, especially EC, may better help understand the mechanism of NFT formation.

Weighted gene co-expression network analysis (WGCNA) is a biology algorithm used to describe the correlation between clinical characters and gene expression based on the microarray data (Langfelder and Horvath, 2008). WGCNA can be used for clustering genes with highly correlated expression, for relating the modules to phenotypes to get the most phenotypic trait-related module, and for summarizing these co-expressed gene clusters by identification of the module eigengene or hub genes. Random forest (RF) is a more advanced machine learning algorithm based on a decision tree (Sarica et al., 2017). Like other decision trees, random forests can be used for both regression and classification.

In this study, we performed ssGSEA, machine learning, and WGCNA analysis on publicly accessible transcriptome data obtained from the human different cortex regions of individuals at different Braak stages. We found the similarities and differences in the transcription patterns of the genome in the three different brain regions [EC, temporal and frontal cortex (TC, FC)] in Braak stages 0–VI. By evaluating the ssGSEA results of EC, we found that the oxidative damage pathway plays a vital role in classifying the Braak stages *via* the random forest and best subset algorithm, the imp is 0.57. Through calculating the correlation coefficients between the modules and the oxidative damage pathway, we obtained a module of interest. We then disclosed the overlapping genes between differentially expressed genes (DEG, between Braak stage 0 and Braak stage I–VI) and genes of interest in the module. Using these overlapping genes, we conducted metascape analysis and further identified the central players within the module through network analysis. Our findings reveal that *CIQA*, *CIQB*, *LYN*, *CD68*, *LAPTM5*, *IFI30*, *PI3KAP1*, *HCK*, and *ARHGDI1B* are significantly associated with oxidative damage and immune response, which may be novel biomarkers involved in AD.

Results

Identification of consensus modules across different cortical regions

Before WGCNA, the genes detected in GSE131617 were filtered according to the filtering procedure described in Method, and 13,629 genes were obtained. Then the microarray

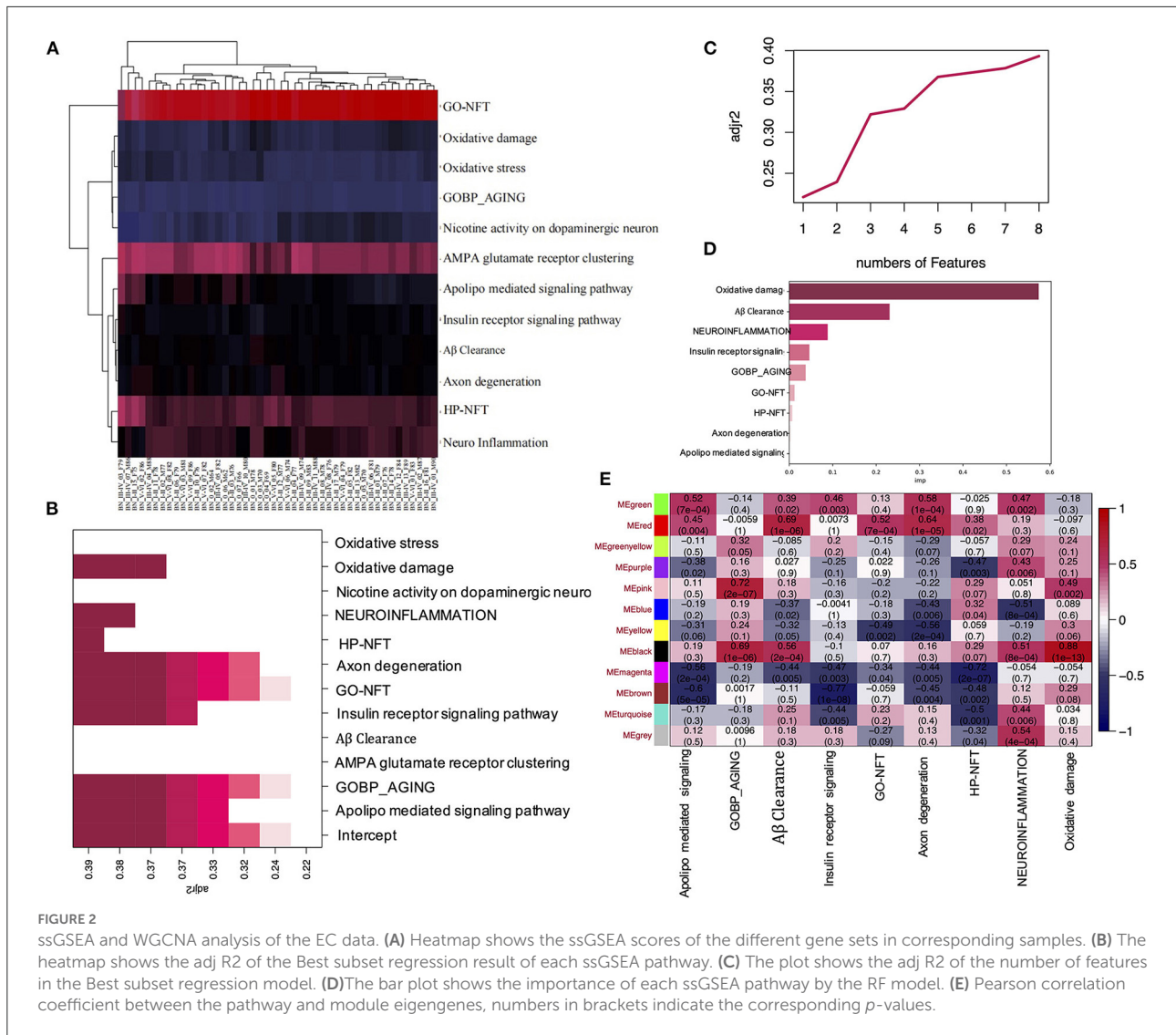
data of 46 samples in each cortical region were read by R for Hierarchical clustering (Supplementary Figure S1a). The consensus network of scale independence and mean connectivity analysis showed that when the weighted value equals to 14, the average degree of connectivity was close to 0, and scale independence was greater than 0.9, so the weighted value was set to 14 (Supplementary Figure S1b). WGCNA was performed to identify consensus modules. A comparison between EC set-specific modules and EC-FC consensus modules of the global co-expression network indicated that most EC modules were preserved in FC (Figure 1A). The strong overlap of the corresponding gene modules showed the similarity of cluster patterns in the EC and FC regions. Figures 1B–G and Supplementary Figures S1c, S2, S3 show that the overall preservation of the three networks is a positive correlation. The mean density of the three networks exceeded 0.9 in all 3 cortical regions, demonstrating that the overall structures of the co-expression networks were similar for the three cortical regions. These results indicated that the differences in these cortical regions may exist in the particular genes within the consensus network.

ssGSEA functional enrichment analyses and key pathway identification and validation help to find the module of interest verified in WGCNA analysis in EC

In the above results, we found that the overall structures of the co-expression networks were similar for the three cortical regions. In addition, an abundance of studies have shown that in the Braak stages I–II, aberrant deposits of NFT first appear in the entorhinal cortex, which is significant for finding the potential biomarkers and therapeutic targets of AD.

To explore the signaling pathways most related to Alzheimer's disease, first, the ssGSEA analysis was performed (Figure 2A). The gene set of pathways related to Alzheimer's disease can be seen in Supplementary Table S1. The second, best subset regression was conducted to identify the representative subset (Figures 2B,C). From the results, we can see that the feature number of best subsets is 8, and GO-NFT, HP-NFT, oxidative damage, and axon degeneration pathway are saved in the best subset. Next, we performed the random forest algorithm based on the sklearn and boruta packages to analyze the best subset of data to find the most important features, as shown in Figure 2D and Supplementary Table S2, the oxidative damage pathway was found to be the most important feature.

To identify the modules which are most significantly associated with the oxidative damage pathway in EC, the Pearson's correlation coefficient between the module and oxidative damage was calculated. The highest positive association in the module trait relationship was found between

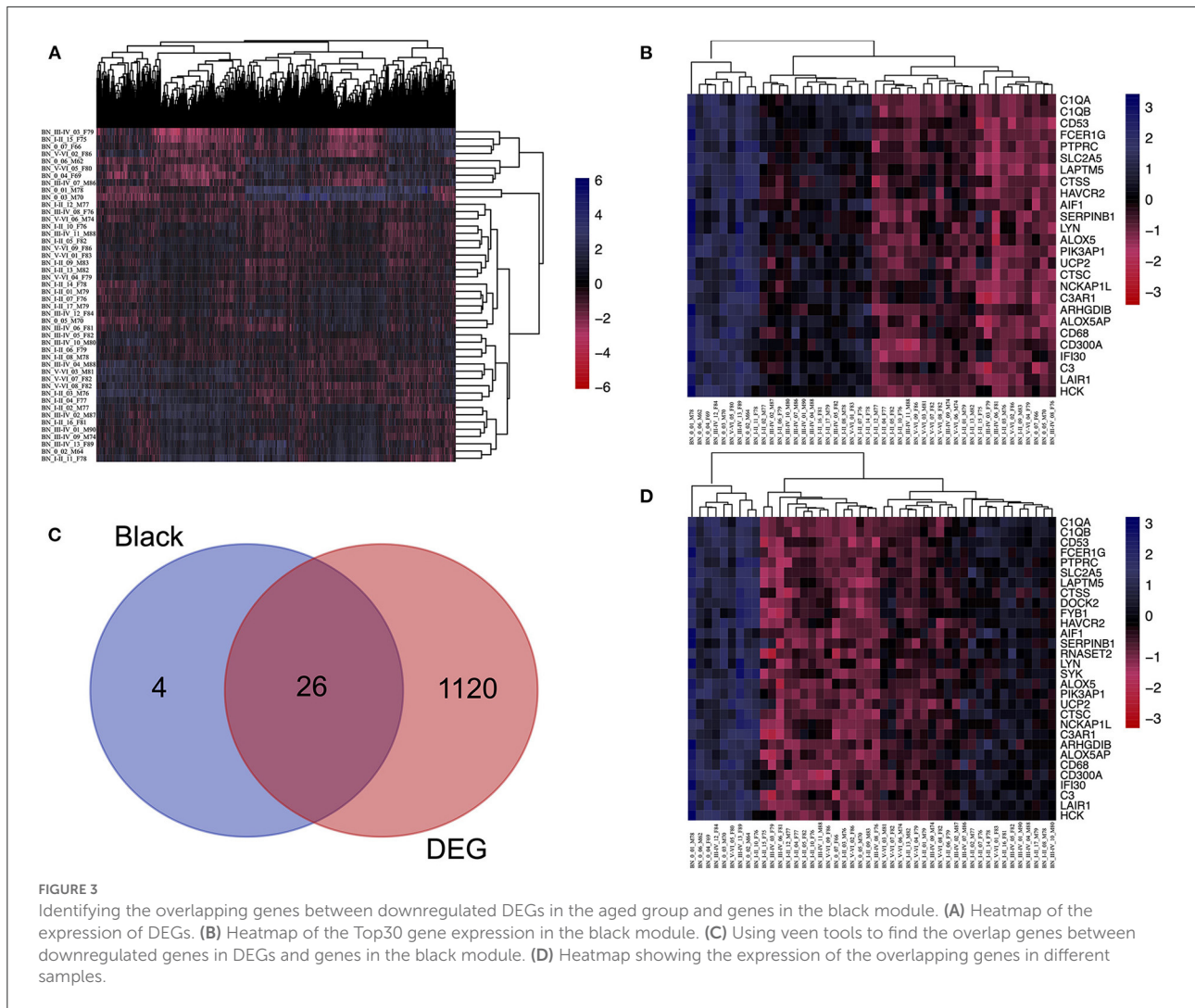


Identifying the hub gene functional annotation

The above-identified overlapping genes were subjected to GO functional and KEGG pathway enrichment analysis. The biological processes of overlapping genes were found to focus on the regulation of inflammatory response and leukocyte degranulation. The molecular functions of overlapping genes were found to focus on IgE binding, non-membrane spanning protein tyrosine kinase activity, and phosphotransferase activity (Figure 4 and Supplementary Figure S7).

Identification of the most significant genes and network construction

To identify the most important genes related to oxidative damage, the overlapping genes were further filtered by RF classification. Gene counts were input into the RF classifier model, and the unimportant genes, such as *CIQA*, *CIQB*, *CTSC*, *SLC2A5*, *UCP2*, and others, were removed (Figure 5A and Supplementary Table S3). To ascertain the significance of genes and analyze the network in the corresponding modules, the PPI maps were constructed via String (Figure 5B). Hub genes

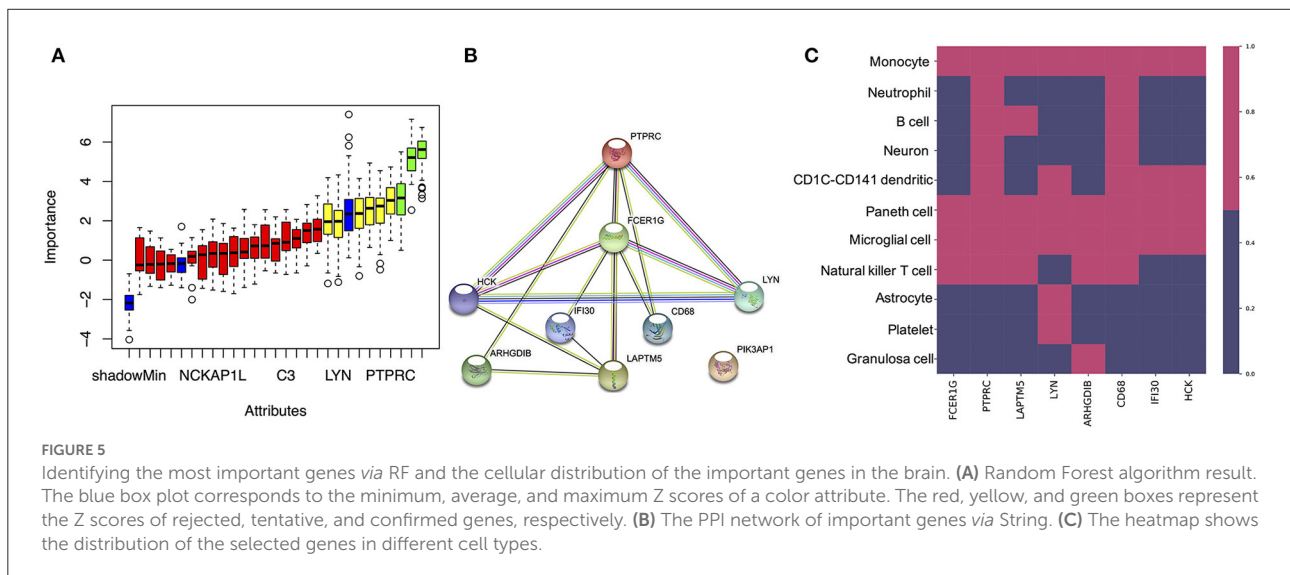
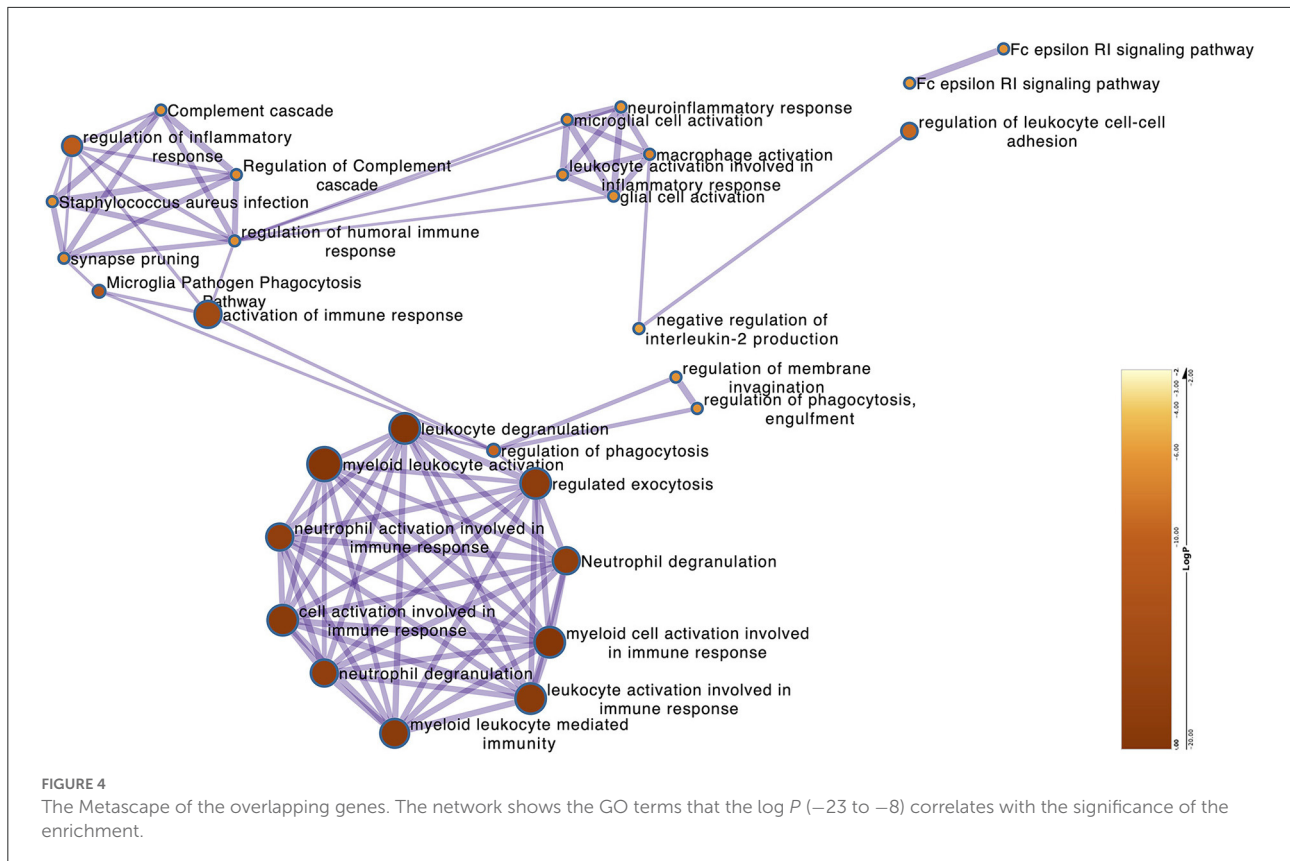


in the network, including *PTPRC*, *LYN*, *LAPYM5*, *HCK*, *IFI30*, *ARHGDI1B*, and *PIK3AP1* were constructed. In the cell marker database, we found that the distribution of the above genes in brain cells was very similar, mainly in microglia cells (Figure 5C).

Discussion

NFT is the major pathological characteristic of neurodegenerative diseases, such as PD (Parkinson’s disease)/AD (Wang and Mandelkow, 2016). Exploring the mechanism of NFT formation is extremely important for discovering the therapeutic targets in these diseases. In this study, we performed WGCNA, ssGSEA, and machine learning analysis on the dataset GSE131617, which includes 46 samples from individuals at Braak stages between 0 and I-VI. Data from multiple samples based on the different brain regions (EC, FC,

TC) is a good candidate for WGCNA analysis. First, consensus modules between different brain regions were constructed, and 7 consensus modules were identified between EC and FC. Figures 1B-G and Supplementary Figures S1c, S2, S3 showed that the overall preservation of the three networks was a positive correlation. The mean density of the three networks exceeded 0.9 in all 3 consensus modules, demonstrating that the overall structures of the co-expression networks were similar for the 3 cortical regions. However, the purple, pink, green-yellow, and magenta module of EC were not recognized in the consensus module (EC, FC), indicating that the difference between the two regions was related to these modules. Furthermore, the black and red modules in EC that are most related to oxidative damage and the $A\beta$ clearance pathway have not been recognized in the consensus module identified by EC and TC (Figure 2E and Supplementary Figure S2). These showed that TC was quite



different from EC in the signal pathway of oxidative damage and $A\beta$ clearance.

A number of studies show that NFT formed by the aggregation of tau is the main pathological character of AD, the peak of tau aggregation occurs in the Braak stages I of

individuals in their 40–50 s, as opposed to in later life (Wischik et al., 2014). Furthermore, many studies have shown that the EC is the region where NFT deposits occur first during the process of neurodegeneration (Cui et al., 2015). Therefore, studying the differences in gene transcription levels between Braak stages I

and Braak Stages 0 in the EC is extremely important to reveal the pathogenesis and therapeutic targets of AD. It should be added that we use the Braak stage as a simple qualitative marker of AD to identify the DEGs between the Braak stage 0 and Braak stage I–VI. In this study, when we performed ssGSEA and random forest analysis on the dataset of EC samples, we found that the unexpected oxidative damage signaling pathway was most important when distinguishing between Braak stage 0 and Braak stages I–VI rather than the signaling pathway related to NFT (Figures 2A–D). This indicates that among the important basis of Braak stages, the formation of NFT is more likely due to changes in the expression level of genes related to the oxidative stress pathway, rather than the NFT signaling pathway. When we analyzed the overlapping genes in the black module which were most related to oxidative damage and the DEG, we found that these genes were not only related to oxidative damage but also related to immune response and microglia-mediated inflammation (Figures 2E, 3, 4). To identify the genes that were most intensively related to Braak stages, we further used one of the machine learning algorithms, Random Forest, and inputted the expression matrix of the overlapping 26 genes as features into the model for training, and finally screened out 9 key genes (Figure 5A and Supplementary Table S3). When analyzing these 9 molecules, we found that most of them are expressed in microglia (Figure 5C), which further indicated that microglia might play an important role in the Braak stages (0 vs. I–VI).

It has been reported that activated microglia can induce the formation of NFT (Fan et al., 2017), and several hypotheses can explain how the activated microglia mediates the formation of NFT, such as complement pathway, IL-CDK5 pathway, and exosome secretion, etc. (Quintanilla et al., 2004; Asai et al., 2015; Saha and Sen, 2019; Vogels et al., 2019). However, this requires further research, examining how molecules such as *LYN*, *HCK*, and *PTPRC*, which are distributed in the microglia, promote the formation of NFT. *LYN* and *HCK*, as Non-receptor tyrosine-protein kinases, can combine with *NLRP3*, which is involved in the phosphorylation of tau and the formation of NFT to promote the release of *IL1B* from microglia (Fitzer-Attas et al., 2000; Jevtic et al., 2017; Gwon et al., 2019; Kong et al., 2020). In the co-expression network, *PTPRC* and *LAPTM5* were identified as hub genes. *PTPRC* is not only an important regulator of T cell and B cell antigen receptor signal transduction but also an enzyme that dephosphorylates *LYN*. It has been reported that *LAPTM5* can not only regulate the production of pro-inflammatory cytokines in macrophages but also regulate the antigen receptor signal transduction of T cells and B cells (Zouali, 2014). There is a lot of data showing that *LAPTM5* and *PTPRC* are not only co-expressed in AD/PD (Figure 5B), but also in systemic lupus erythematosus, lung cancer, and other diseases (Salih et al., 2019; Zhang et al., 2020, 2021). This indicated that *LAPTM5* and *PTPRC* may play a similar role in the phosphorylation of *LYN*. Moreover, in this study, we found that a decrease in the expression of these co-expressed genes at Braak stage I–VI, which was negatively correlated with the degree of NFT needs

further discussion. It has been reported that the expression of *LYN* in activated microglia is less than that of homeostasis microglia (Sierksma et al., 2020). This indicated that *LYN* may play a role in activated microglia, and the decrease of *PTPRC* and *LAPTM5* may lead to an increase of phosphorylated *LYN* so that it can promote the release of inflammatory factors.

In this study, we also found that *IFI30* and *FCER1G* in the co-expression network were also distributed in microglia (Figures 5B,C). It has been reported that both of them are highly expressed in microglia around $A\beta$ (Satoh et al., 2018), which may imply that the two of them are involved in the function of $A\beta$ clearance (Figure 2E). However, in this study, we found that their expression in Braak stage I–VI decreased. How their reduction in microglia promotes the formation of NFT requires further study.

To our surprise, *ARHGDI1B* was found to be mainly co-expressed with *LAPTM5* and *PTPRC* in the co-expression network. Its related pathways are involved in the GPCR signaling pathway, apoptosis, and survival Caspase cascade (Kardol-Hoefnagel et al., 2020). Through network analysis (Figures 5B,C), we speculated that it may have similar functions to *LAPTM5* and *PTPRC*. A decrease in the expression of *ARHGDI1B* may also play a role in the formation of NFT. Further studies are needed to reveal the function of *ARHGDI1B* in microglia.

In conclusion, through WGCNA and machine learning analysis, we found that the EC, FC, and TC regions of Braak stages 0–VI had similar genome transcription patterns. Furthermore, we found that oxidative stress might play a key role in the development of AD, which may be mediated by *ARHGDI1B*, *IFI30*, and *LAPTM5*, etc. through microglia.

Materials and methods

Data acquisition and preprocessing

The data used in this paper were obtained from the GEO database in NCBI (Gene Expression Omnibus, <http://www.ncbi.nlm.nih.gov/geo>), and the data entry number is GSE131617 (Kikuchi et al., 2020, p. 1). The platform is Affymetrix Human Exon 1.0 ST Array [transcript (gene) version, HuEx-1_0-st]. Gene expression in the cortex of Braak stages 0, I–II, III–IV, and V–VI was detected. The normalized and log₂-transformed data from 71 samples were downloaded and the expression matrix was obtained, and data filtering was performed before WGCNA analysis. For data filtering, first, 61 samples with a neuropathological diagnosis of minimal senile change and AD were performed. Second, the gene type of *APOE* was 3*3 and 15 samples were removed. Forty six samples in the dataset were kept and the clinical characteristics of these samples are shown in Supplementary Table S4. Probes without corresponding annotation information were removed. There were about 13,629 genes in the dataset.

Single sample gene set enrichment analysis

ssGSEA is an implementation method proposed for a single sample GSEA (Subramanian et al., 2005; Barbie et al., 2009). The difference between GSEA and ssGSEA is that ssGSEA does not need to prepare an expression matrix file. The functions of the gene set were acquired from a Molecular Signatures Database (MSigDB) as described in the review, including aging, insulin receptor pathways, oxidative stress, oxidative damage, NFT, and Nicotine activity on dopaminergic neurons, etc. The performances of the pathway in the gene set were quantified by the ssGSEA algorithm (R package “gsva”) based on transcriptome profiling data and pathway gene sets.

Application of best subset regression to find the best subset of the ssGSEA pathway

The entorhinal cortical samples were grouped into individuals of Braak stage 0 and Braak stages I–VI. We used the Braak stage as a binary category for simple AD diagnosis and classification. Inputting the ssGSEA scores into the best subset regression model *via* leaps package to predict which group the samples belong to, and the best number of features as the input for subsequent analysis.

Application of random forest algorithm to find the most important pathway and genes related to braak stages

The entorhinal cortical samples were grouped into individuals of Braak stage 0 or individuals of Braak stages I–VI. Inputting the overlapping genes counts and ssGSEA enrich scores into the random forest classifier model *via* Boruta package to predict which group the samples belonged to and the most important overlapping genes and identify the ssGSEA pathway for the most accurate model for grouping.

Construction of weighted gene co-expression network and identification of significant modules

Data were processed using R 3.4.2 software. To ensure that the results of network construction are reliable, abnormal samples were removed. Then, the weighted gene co-expression network was constructed by the WGCNA package based on R 3.4.2. First, the Pearson correlation coefficient was calculated to assess the similarity of the gene expression profiles. Second,

the correlation coefficients between genes were weighted by a power function to obtain a scale-free network. A gene module is a cluster of densely interconnected genes in terms of co-expression. Then, the hierarchical cluster was used to identify gene modules and different modules were represented by different colors. The dynamic treecut method was used to identify different modules, the adjacency matrix was converted to a topology overlay matrix (TOM) and modules were detected by cluster analysis during module selection.

Correlation analysis of gene modules with clinical phenotype

To detect the associations of modules and clinical phenotype (ssGSEA scores), first, the clinical phenotype data and gene expression data were correlated using the match function. Secondly, the associations of the module eigengene (ME) and the clinical phenotype were calculated by Pearson’s correlation analysis. Modules showing significant association to oxidative damage pathway were obtained. At last, to further confirm the modules with significant correlation to oxidative damage, the correlation coefficient between the module membership (gene expression level) with gene significance (GS, for assessing the association of genes with phenotypes) was calculated using the labeled heatmaps function, and *p*-values were obtained.

Finding the overlapping genes between the differentially expressed genes (DEG, between braak stage 0 and braak stages I–VI) and genes of interest in the module verified by WGCNA

The entorhinal cortical samples were grouped into individuals at Braak stages 0 and individuals at Braak stages I–VI and Limma packages were performed to find the DEG (Diboun et al., 2006; Ritchie et al., 2015). Samples of Braak stage 0 were regarded as control, 201 genes with a corrected *p*-value of less than 0.05 were found in samples of Braak stages I–VI. Next, the overlapping genes between downregulated DEG and genes of interest in the module were discovered by using online venn tools (<http://bioinformatics.psb.ugent.be/webtools/Venn/>).

Metascape analyzes, identification of hub genes, and protein-protein interaction analysis

For the obtained overlapping genes, functional enrichment of Gene Ontology (GO) and KEGG pathways analyses were performed using Metascape (<https://metascape.org>) (Zhou et al.,

2019). Log P between -23 and -8 were considered to be significant enrichment. These enrichment results were also analyzed using Cytoscape for the identification of important pathways (Warde-Farley et al., 2010). The identified hub genes were further confirmed and analyzed using a String network constructed by the online database String (<http://string-db.org>) (Szkłarczyk et al., 2017).

Exploring the cellular distribution of the identified genes

By using the Cell marker database (<http://biocc.hrbmu.edu.cn/CellMarker/search.jsp>), the cellular distribution of the identified important genes was further explored.

Data availability statement

The datasets presented in this study can be found in online repositories. The names of the repository/repositories and accession number(s) can be found in the article/Supplementary Material.

Author contributions

KC: conceptualization, methodology, investigation, data curation, visualization, and writing—original draft. XZ: conceptualization, investigation, and writing—original draft. HT and GW: software. HG: resources and software. WY: data curation. SC: supervision. FW, DS, and JL: supervision and

writing—review and editing. All authors contributed to the article and approved the submitted version.

Acknowledgments

We acknowledge the GEO database for providing their platforms and contributors for uploading meaningful datasets.

Conflict of interest

The authors declare that the research was conducted in the absence of any commercial or financial relationships that could be construed as a potential conflict of interest.

Publisher's note

All claims expressed in this article are solely those of the authors and do not necessarily represent those of their affiliated organizations, or those of the publisher, the editors and the reviewers. Any product that may be evaluated in this article, or claim that may be made by its manufacturer, is not guaranteed or endorsed by the publisher.

Supplementary material

The Supplementary Material for this article can be found online at: <https://www.frontiersin.org/articles/10.3389/fnagi.2022.837770/full#supplementary-material>

References

- Asai, H., Ikezu, S., Tsunoda, S., Medalla, M., Luebke, J., Haydar, T., et al. (2015). Depletion of microglia and inhibition of exosome synthesis halt tau propagation. *Nat. Neurosci.* 18, 1584–1593. doi: 10.1038/nn.4132
- Barbie, D. A., Tamayo, P., Boehm, J. S., Kim, S. Y., Moody, S. E., Dunn, I. F., et al. (2009). Systematic RNA interference reveals that oncogenic KRAS-driven cancers require TBK1. *Nature* 462, 108–112. doi: 10.1038/nature08460
- Braak, H., and Braak, E. (1991). Neuropathological staging of Alzheimer-related changes. *Acta Neuropathol.* 82, 239–259. doi: 10.1007/BF00308809
- Cui, S., Sun, H., Gu, X., Lv, E., Zhang, Y., Dong, P., et al. (2015). Gene expression profiling analysis of locus coeruleus in idiopathic Parkinson's disease by bioinformatics. *Neurol. Sci.* 6, 97–102. doi: 10.1007/s10072-015-2304-0
- Diboun, I., Wernisch, L., Orengo, C. A., and Koltzenburg, M. (2006). Microarray analysis after RNA amplification can detect pronounced differences in gene expression using limma. *BMC Genomics* 7, 252. doi: 10.1186/1471-2164-7-252
- Dickson, D. W. (1997). Neurodegenerative diseases with cytoskeletal pathology: a biochemical classification. *Ann. Neurol.* 42, 541–544. doi: 10.1002/ana.410420403
- Duyckaerts, C., Bannicib, M., Grignon, Y., Uchiyama, T., He, Y., Piette, F., et al. (1997). Modeling the relation between neurofibrillary tangles and intellectual status. *Neurobiol. Aging* 18, 267–273. doi: 10.1016/S0197-4580(97)80306-5
- Fan, Z., Brooks, D. J., Okello, A., and Edison, P. (2017). An early and late peak in microglial activation in Alzheimer's disease trajectory. *Brain* 140, 792–803. doi: 10.1093/brain/aww349
- Fitzner-Attas, C. J., Lowry, M., Crowley, M. T., Finn, A. J., Meng, F., DeFranco, A. L., et al. (2000). Fcγ receptor-mediated phagocytosis in macrophages lacking the Src family tyrosine kinases Hck, Fgr, and Lyn. *J. Exp. Med.* 191, 669–682. doi: 10.1084/jem.191.4.669
- Grober, E., Dickson, D., Sliwinski, M. J., Buschke, H., Katz, M., Crystal, H., et al. (1999). Memory and mental status correlates of modified Braak staging. *Neurobiol. Aging* 20, 573–579. doi: 10.1016/S0197-4580(99)00063-9
- Gwon, Y., Kim, S.-H., Kim, H. T., Kam, T.-I., Park, J., Lim, B., et al. (2019). Amelioration of amyloid β-FcγRIIb neurotoxicity and tau pathologies by targeting LYN. *FASEB J.* 33, 4300–4313. doi: 10.1096/fj.201800926R
- Jevtic, S., Sengar, A. S., Salter, M. W., and McLaurin, J. (2017). The role of the immune system in Alzheimer disease: etiology and treatment. *Ageing Res. Rev.* 40, 84–94. doi: 10.1016/j.arr.2017.08.005
- Kardol-Hoefnagel, T., van Logtestijn, S. A. L. M., and Otten, H. G. (2020). A Review on the Function and Regulation of ARHGDI2/RhoGDI2 expression including the hypothetical role of ARHGDI2/RhoGDI2 autoantibodies in kidney transplantation. *Transplant Direct* 6, e548. doi: 10.1097/TXD.0000000000000993
- Kikuchi, M., Sekiya, M., Hara, N., Miyashita, A., Kuwano, R., Ikeuchi, T., et al. (2020). Disruption of a RAC1-centred network is associated with Alzheimer's disease pathology and causes age-dependent neurodegeneration. *Hum. Mol. Genet.* 29, 817–833. doi: 10.1093/hmg/ddz320

- Kong, X., Liao, Y., Zhou, L., Zhang, Y., Cheng, J., Yuan, Z., et al. (2020). Hematopoietic cell kinase (HCK) is essential for NLRP3 inflammasome activation and lipopolysaccharide-induced inflammatory response *in vivo*. *Front. Pharmacol.* 11, 581011. doi: 10.3389/fphar.2020.581011
- Langfelder, P., and Horvath, S. (2008). WGCNA: an R package for weighted correlation network analysis. *BMC Bioinformatics* 9, 559. doi: 10.1186/1471-2105-9-559
- Nakamura, A., Kaneko, N., Villemagne, V. L., Kato, T., Doecke, J., Doré, V., et al. (2018). High performance plasma amyloid- β biomarkers for Alzheimer's disease. *Nature* 554, 249–254. doi: 10.1038/nature25456
- Quintanilla, R. A., Orellana, D. I., González-Billault, C., and Maccioni, R. B. (2004). Interleukin-6 induces Alzheimer-type phosphorylation of tau protein by deregulating the cdk5/p35 pathway. *Exp. Cell Res.* 295, 245–257. doi: 10.1016/j.yexcr.2004.01.002
- Ritchie, M. E., Phipson, B., Wu, D., Hu, Y., Law, C. W., Shi, W., et al. (2015). limma powers differential expression analyses for RNA-sequencing and microarray studies. *Nucleic Acids Res.* 43, e47. doi: 10.1093/nar/gkv007
- Saha, P., and Sen, N. (2019). Tauopathy: a common mechanism for neurodegeneration and brain aging. *Mech. Ageing Dev.* 178, 72–79. doi: 10.1016/j.mad.2019.01.007
- Salih, D. A., Bayram, S., Guelfi, S., Reynolds, R. H., Shoai, M., Ryten, M., et al. (2019). Genetic variability in response to amyloid beta deposition influences Alzheimer's disease risk. *Brain Commun.* 1, fcz022. doi: 10.1093/braincomms/fcz022
- Sarica, A., Cerasa, A., and Quattrone, A. (2017). Random forest algorithm for the classification of neuroimaging data in Alzheimer's disease: a systematic review. *Front. Aging Neurosci.* 9, 329. doi: 10.3389/fnagi.2017.00329
- Satoh, J.-I., Kino, Y., Yanaizu, M., Ishida, T., and Saito, Y. (2018). Microglia express gamma-interferon-inducible lysosomal thiol reductase in the brains of Alzheimer's disease and Nasu-Hakola disease. *Intractable Rare Dis. Res.* 7, 251–257. doi: 10.5582/irdr.2018.01119
- Sierksma, A., Lu, A., Mancuso, R., Fattorelli, N., Thrupp, N., Salta, E., et al. (2020). Novel Alzheimer risk genes determine the microglia response to amyloid- β but not to TAU pathology. *EMBO Mol. Med.* 18. doi: 10.15252/emmm.201910606
- Solomon, A., Mangialasche, F., Richard, E., Andrieu, S., Bennett, D. A., Breteler, M., et al. (2014). Advances in the prevention of Alzheimer's disease and dementia. *J. Intern. Med.* 275, 229–250. doi: 10.1111/joim.12178
- Subramanian, A., Tamayo, P., Mootha, V. K., Mukherjee, S., Ebert, B. L., Gillette, M. A., et al. (2005). Gene set enrichment analysis: a knowledge-based approach for interpreting genome-wide expression profiles. *Proc. Natl. Acad. Sci. U.S.A.* 102, 15545–15550. doi: 10.1073/pnas.0506580102
- Szklarczyk, D., Morris, J. H., Cook, H., Kuhn, M., Wyder, S., Simonovic, M., et al. (2017). The STRING database in 2017: quality-controlled protein-protein association networks, made broadly accessible. *Nucleic Acids Res.* 45, D362–D368. doi: 10.1093/nar/gkx937
- Vogels, T., Murgoci, A.-N., and Hromádka, T. (2019). Intersection of pathological tau and microglia at the synapse. *Acta Neuropathol. Commun.* 7, 109. doi: 10.1186/s40478-019-0754-y
- Wang, Y., and Mandelkow, E. (2016). Tau in physiology and pathology. *Nat. Rev. Neurosci.* 17, 5–21. doi: 10.1038/nrn.2015.1
- Warde-Farley, D., Donaldson, S. L., Comes, O., Zuberi, K., Badrawi, R., Chao, P., et al. (2010). The GeneMANIA prediction server: biological network integration for gene prioritization and predicting gene function. *Nucleic Acids Res.* 38, W214–220. doi: 10.1093/nar/gkq537
- Wischnik, C. M., Harrington, C. R., and Storey, J. M. D. (2014). Tau-aggregation inhibitor therapy for Alzheimer's disease. *Biochem. Pharmacol.* 88, 529–539. doi: 10.1016/j.bcp.2013.12.008
- Zhang, L., Zhang, M., Chen, X., He, Y., Chen, R., Zhang, J., et al. (2020). Identification of the tubulointerstitial infiltrating immune cell landscape and immune marker related molecular patterns in lupus nephritis using bioinformatics analysis. *Ann. Transl. Med.* 8, 18. doi: 10.21037/atm-20-7507
- Zhang, T., Yang, H., Sun, B., and Yao, F. (2021). Four hub genes regulate tumor infiltration by immune cells, antitumor immunity in the tumor microenvironment, and survival outcomes in lung squamous cell carcinoma patients. *Aging* 13, 3819–3842. doi: 10.18632/aging.202351
- Zhou, Y., Zhou, B., Pache, L., Chang, M., Khodabakhshi, A. H., Tanaseichuk, O., et al. (2019). Metascape provides a biologist-oriented resource for the analysis of systems-level datasets. *Nat. Commun.* 10, 1523. doi: 10.1038/s41467-019-09234-6
- Zouali, M. (2014). Transcriptional and metabolic pre-B cell receptor-mediated checkpoints: implications for autoimmune diseases. *Mol. Immunol.* 62, 315–320. doi: 10.1016/j.molimm.2014.01.009